HHS Public Access

Author manuscript

Cryst Growth Des. Author manuscript; available in PMC 2021 July 01.

Published in final edited form as:

Cryst Growth Des. 2020 July ; 20(7): 4335–4345. doi:10.1021/acs.cgd.0c00020.

Polymer-Assisted Aripiprazole-Adipic Acid Cocrystals Produced by Hot Melt Extrusion Techniques

Arun Butreddy[1], **Sandeep Sarabu**[1], **Suresh Bandari**[1], **Nagireddy Dumpa**[1], **Feng Zhang**[2], **Michael A. Repka**[1,3,*]

[1]Department of Pharmaceutics and Drug Delivery, School of Pharmacy, The University of Mississippi, University, MS 38677, USA

[2]College of Pharmacy, The University of Texas at Austin, Austin, TX 78712, USA

[3]Pii Center for Pharmaceutical Technology, The University of Mississippi, University, MS 38677, USA

Abstract

Pharmaceutical cocrystals are a promising strategy to increase the solubility and dissolution rate of poorly soluble drugs. However, their manufacturing process requires a large quantity of solvents. The present study aimed to produce cocrystals by a solvent-free hot melt extrusion (HME) method to improve their solubility and dissolution rate. Aripiprazole (ARP) and adipic acid (ADP) were used as a weakly basic drug and acidic coformer, respectively. The processability of a plain ARP-ADP physical mixture (PM) compared with a PM with 5% Soluplus® (SOL) was investigated. Incorporating 5% SOL into the ARP-ADP blend reduced the processing torque and improved processability. The effects of temperature and screw speed on the formation of cocrystals were studied, and cocrystals were characterized by differential scanning calorimetry (DSC), fourier transform infrared (FTIR) spectroscopy, nuclear magnetic resonance (NMR) spectroscopy, powder X-ray diffraction (PXRD), scanning electron microscopy, and hot-stage microscopy. FTIR spectra revealed noncovalent interaction between ARP and ADP, which was confirmed by NMR spectra. Similarly, PXRD data exhibited characteristic peaks confirming the formation of new crystalline material. Further, the results indicated that cocrystals demonstrated higher dissolution rates and improved compressibility, as well as enhanced flow characteristics compared with pure ARP, suggesting its suitability in the development of solid dosage forms.

Graphical Abstract

[*]**Corresponding Author** Michael A. Repka, D.D.S., Ph.D., Distinguished Professor and Chair, Department of Pharmaceutics and Drug Delivery Director, Pii Center for Pharmaceutical Technology, School of Pharmacy, The University of Mississippi, University, MS 38677, Phone: 662-915-1155, Fax: 662-915-1177, marepka@olemiss.edu.

Author Contributions

Arun Butreddy, Sandeep Sarabu, Suresh Bandari, and Michael Repka designed the study. Arun Butreddy, Sandeep Sarabu, Nagireddy Dumpa, performed the experiments and analyzed data. Feng Zhang performed the XRD analysis. Arun Butreddy wrote the manuscript. Initial review and editing by Bandari, S.; Supervision and manuscript editing by M.A. Repka. The authors agreed to be accountable for all aspects of the work, ensuring that questions related to the accuracy or integrity of any part of the work are appropriately investigated and resolved. All authors have given approval to the final version of the manuscript.

No competing financial interest.

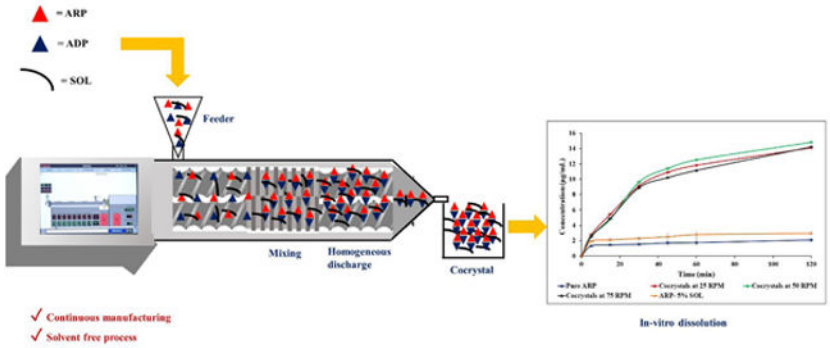

Schematic representation of polymer assisted ARP-ADP cocrystals via hot melt extrusion technique.

INTRODUCTION

Approximately 90% of new chemical entities in the pipeline and 40% of the marketed drugs are reported to have poor aqueous solubility.[1,2] Therefore, formulation approaches to enhance the solubility and dissolution rate of poorly soluble drugs play a crucial role in improving the oral bioavailability. Different formulation strategies such as amorphous solid dispersions, cocrystals, complexation, nanonization and lipid-based drug delivery systems have been explored to improve the dissolution rate and bioavailability of poorly soluble drugs.[3–7] Among these strategies, cocrystals is one of the effective approach to modify the physicochemical properties of APIs such as solubility, physical stability and mechanical properties without altering the physiological or chemical action of the drug substances.[4,8] Pharmaceutical cocrystals are crystalline materials comprised of an active pharmaceutical ingredient (API) and a coformer, bound together by noncovalent interactions such as hydrogen bonds, van der Waals forces, or π-bonds.[9]

Traditional methods have been used in the synthesis of pharmaceutical cocrystals including solution, slurry crystallization and liquid or milling assisted grinding.[10,11] However, these techniques have been extensively used in the screening of cocrystals.[12,13] Utilization of these techniques is time-consuming, difficult to scale up, and most of them require organic solvents, which may leave residual solvent impurities in the cocrystals.[14] In the recent years, the advanced techniques such as ultrasonication, supercritical fluid, microfluidic anti-solvent, thermal ink-jet printing and hot melt extrusion techniques have been employed for cocrystals synthesis.[15–19] Despite the advancement of these techniques, a further understanding and optimization of the process is needed for successful scale-up.

Hot melt extrusion (HME) is a one-step, continuous, scalable, and industrially feasible process to develop cocrystals.[20,21] Recently, use of HME as a continuous process to develop and manufacture cocrystals has gained interest in the field of pharmaceutical research.[4,22] High throughput, low residence time, lack of organic solvents, and a combination of intense mixing and controlled temperature make the HME process more efficient in producing cocrystals than other traditional technologies.

Aripiprazole (ARP, Figure 1) is an atypical antipsychotic agent used to treat schizophrenia. It is a weakly basic drug with a pKa of 7.6 and a melting point of 139°C.[23] ARP is a class II drug according to the biopharmaceutics classification system, with an aqueous solubility of 0.007 mg/mL.[24] Thus, solubility and dissolution are rate-limiting steps in the absorption and bioavailability of ARP. The coformer, adipic acid (ADP), is a dicarboxylic acid derivative with a melting point of 155°C.[25] ADP has been used as a coformer with isoniazid[26] and pyrazinamide.[25]

The preparation of ARP cocrystals with phenolic coformers (namely resorcinol, catechol, hydroquinone, pyrogallol, and phloroglucinol) using slow evaporation and solid-state grinding methods has been reported. In previous reports, authors have mainly focused on establishing a melting point correlation between ARP and cocrystals with phenolic coformers.[27] Cho *et al*.[28] investigated the formation of ARP cocrystals with catechol, resorcinol, phloroglucinol, and orcinol. They reported that ARP cocrystals prepared using neat and liquid-assisted grinding methods showed an improved dissolution profile compared with pure ARP.

The novelty of the current investigation lays in the exploration of the feasibility of producing ARP cocrystals by HME using ADP as a coformer, to investigate the effect of Soluplus® (SOL) on cocrystal formation, and to study the effects of temperature and screw speed on ARP-ADP cocrystal formation. The ARP-ADP cocrystals produced by HME were characterized by differential scanning calorimetry (DSC), powder X-ray diffraction (PXRD), hot-stage microscopy (HSM), scanning electron microscopy (SEM), fourier transform infrared spectroscopy (FTIR), nuclear magnetic resonance spectroscopy (NMR), *in vitro* dissolution studies, and their feasibility to formulate solid dosage forms.

EXPERIMENTAL SECTION

Materials

Aripiprazole was obtained from Nexconn Pharmatechs, Ltd. (Tseung Kwan O, Hong Kong), adipic acid was purchased from Spectrum Quality Products, Inc. (Gardena, California, USA), and Soluplus® was generously supplied by BASF Corp. (Florham Park, New Jersey, USA). All other chemicals used were of analytical reagent grade and were used without further purification.

Preparation of ARP-ADP cocrystals

Liquid-assisted grinding—Physical mixtures (PMs) of ARP and ADP at a 1:1 molar ratio were blended with 100 μL of acetonitrile and manually ground by mortar and pestle for 20 min. The obtained sample was analyzed by DSC to determine the formation of cocrystals.

HME processing—HME processing was conducted using a co-rotating twin screw 11-mm extruder (Process 11, Thermo Fisher Scientific, Waltham, Massachusetts, USA) with a length-to-diameter ratio of 40:1. An equimolar ratio of plain ARP and ADP with 5% SOL was passed through a US #30 mesh screen and mixed at 25 rpm for 10 min using a Maxiblend™ blender (GlobePharma, New Brunswick, New Jersey, USA).

Physical mixtures were fed into the extruder at a rate of 0.4 g/min using a volumetric feeder at different extruder barrel temperatures (100°C, 115°C, and 125°C) and at screw speeds of 25, 50, and 75 rpm, and torque was monitored continuously during extrusion. The screw configurations used in the extrusion process are shown in Figure 2. After processing, the extrudates were milled in a mortar and passed through a US #25 mesh sieve with a 700-μm aperture, and subsequently stored in a tightly closed glass vial in a vacuum desiccator at room temperature until further analysis.

Characterization of ARP-ADP cocrystals

DSC analysis—The formation of cocrystals was determined by DSC analysis. DSC thermograms of pure components and extrudates were recorded using a Discovery 25 differential scanning calorimeter (TA Instruments, Newcastle, Delaware, USA) equipped with a RCS90 refrigerator cooling system. Samples of approximately 6 to 8 mg were sealed in an aluminum pan, and an empty aluminum pan was used as a reference. To ensure an inert atmosphere during measurements, samples were equilibrated for 1 min at 25°C and then heated to 200°C at a heating rate of 10°C/min under a nitrogen purge of 50 mL/min.

HSM analysis—HSM analysis was conducted with a Cary 620 IR optical microscope (Agilent, Santa Clara, California, USA) equipped with an electronically controlled hot stage (T95 LinkPad and FTIR 600, Linkam, Epsom, Tadworth, UK). The ARP and cocrystal samples were mounted on glass slips, placed on the hot-stage furnace, and heated to 180°C at a rate of 10°C/min. Changes in sample morphology during heating were recorded as images using Linkam software.

FTIR and chemical imaging analysis—FTIR spectra of pure ARP, ADP, and ARP-ADP cocrystals were obtained with a Cary 660 FTIR Spectrometer (Agilent Technologies, Santa Clara, California, USA) equipped with a MIRacle ATR (Pike Technologies, Madison, Wisconsin, USA) fitted with a single-bounce, diamond-coated ZnSe internal reflection element. A small sample was placed on the crystal surface and pressed using the built-in pressure tower to obtain uniform solid–crystal contact. The spectra were recorded in absorbance mode in the range of 600 to 4000 cm^{-1} with 16 scans and 4 cm^{-1} resolutions. An infrared microscope (Agilent Technologies, Santa Clara, California, USA) equipped with a 64 × 64 focal plane array detector and germanium micro ATR sampling accessory was used to collect the chemical images. Images were recorded at a field of view of approximately 70 × 70 μm and a spatial resolution of 1.1 μm.

PXRD measurement—PXRD was performed to confirm the formation of cocrystals. The diffractograms of pure ARP, ADP, and ARP-ADP cocrystals were recorded at room temperature using the Rigaku X-ray system (D/MAX-2500PC, Rigaku Corp., Tokyo, Japan) using Cu rays (λ = 1.54056 A°) with a voltage of 40 kV and a current of 40 mA, over a 2θ scanning range of 2° to 50°, with a step width of 0.02°/S and a scan speed of 2°/min.

^{1}H and ^{13}C solution-phase NMR—^{1}H and ^{13}C NMR spectra of ARP, ADP, and the cocrystals were obtained on a Bruker Avance spectrometer (Bruker, Rossendorf, Dresden,

Germany) operating at 500 MHz, with dimethyl sulfoxide as a solvent at a concentration of 10mg/mL and tetramethylsilane as an internal standard.

SEM analysis—Shape and surface morphology of the ARP, ADP, and ARP-ADP cocrystals were determined by SEM analysis. The samples were mounted on aluminum stubs using carbon adhesive film, gold-coated with a Hummer® 6.2 sputtering system (Anatech Ltd., Battlecreek, Michigan, USA), and placed in a high-vacuum evaporator to increase the conductivity of the samples. The samples were examined at acceleration potentials of 1.0 to 5.0 kV (JEOL JSM-5600; JEOL, Inc.; Peabody, Massachusetts, USA).

Solubility and *in-vitro* dissolution studies—Solubility studies of ARP and cocrystals were performed by Higuchi and Connors (shake flask) method. Excess amount of the ARP and its cocrystals were added to a vial containing 5mL of DI water and agitated at 500 rpm, 25°C for 48 h using bench mark shaker (Benchmark Scientific Inc, New Jersey, USA). The samples were subsequently centrifuged for 5 min at 13000 rpm to separate the undissolved drug. The supernatant was diluted suitably, and the absorbance was measured at a wavelength of 254 nm by an UV-Vis spectrophotometer (GENESYS™ 180, Thermo Fisher Scientific, Waltham, Massachusetts, USA).

Dissolution studies of pure ARP, ARP-5%SOL and ARP-ADP cocrystals were conducted in 900 mL of DI water using USP apparatus type II (SR8-plus™, Hanson, Chatsworth, California, USA). The temperature of the media was maintained at 37 ± 0.5°C with a paddle speed of 50 rpm for 2 h. Pure ARP, ARP-5%SOL and cocrystal formulations equivalent to 30 mg of ARP were weighed and poured into a hard gelatin capsule (size 0) and placed in dissolution media. Three-milliliter samples were collected at 15, 30, 45, 60, 90, and 120 min and replaced with 3 mL of fresh medium maintained at 37 ± 0.5°C. The samples were filtered through a 10-μm filter (Quality Lab Accessories LLC, Pennsylvania, USA) and diluted suitably. The ARP content was estimated against blank dissolution medium by UV spectrophotometry at an absorbance of 254 nm.

Drug content analysis—Cocrystals equivalent to 30 mg of ARP were weighed and dissolved in methanol, sonicated for 30 min, and centrifuged. The supernatant was collected, filtered, and diluted suitably, and the ARP content in the cocrystals was analyzed using a UV-visible spectrophotometer.

Flow properties (bulk and tapped density measurement)—Three grams each of pure ARP and cocrystal formulations were placed in a 10-mL graduated cylinder, and the volume was recorded. The cylinder was tapped on a flat surface from a height of approximately 2 cm, and the powder volume was measured after 100 taps. The process was repeated until the difference between two consecutive volume readings was less than 2.0%. [29] The bulk and tapped densities were calculated from the weight, bulk and tapped volumes of respective pure ARP and cocrystal formulations. Each measurement was performed in triplicate. The Carr's index (CI) and Hausner ratio (HR) of ARP and the ARP-ADP cocrystals were calculated using equations (1) and (2).

$$CI = \frac{\rho_{tap} - \rho_{bulk}}{\rho_{bulk}} \times 100 \quad (1)$$

$$HR = \frac{\rho_{tap}}{\rho_{bulk}} \quad (2)$$

where ρ_{tap} indicates the tap density and ρ_{bulk} is the bulk density.

True density measurement—The true densities of pure ARP and ARP-ADP cocrystals were determined using a helium pycnometer (AccuPyc II 1340, Micromeritics, Norcross, Georgia, USA). An accurately weighed pure ARP, cocrystals (1–2g) was placed into an empty sample cup. The sample volume was calculated by measuring the pressure in the sample chamber filled with high purity helium gas, and the measurements were repeated for ten cycles.

RESULTS AND DISCUSSION

Cocrystal formation by liquid-assisted grinding

DSC analysis of ARP and ADP cocrystals prepared by liquid-assisted grinding showed a single endothermic melting peak at 128°C. The presence of a distinct single endothermic peak suggests interaction between ARP and ADP components and the formation of ARP-ADP cocrystals. The formation of cocrystals by liquid-assisted grinding indicates the feasibility of cocrystallization with the selected components. This preliminary cocrystals formation with the liquid assisted grinding method suggested the selection of HME process temperature. The barrel temperature in the HME process is a primary experimental parameter that can affect the cocrystal formation. Based on the observations from the literature, it was reported that the extrusion process was successful and better quality cocrystals were formed when the extrusion temperature was set close to that of the cocrystals formation temperature.[4,30,31] The optimal process temperature together with mechanical shear provided by HME is critical for cocrystal formation. In this study, the extrusion temperature was selected in the range of 100–125°C based on the cocrystals formation at 128°C in the liquid assisted grinding method. Selection of temperature range less than the melting temperature of cocrystals, would facilitate the cocrystalization during the extrusion process.

HME processing

Initial extrusion trials were conducted using the Thermo Fisher standard screw configuration, which consists of three mixing zones (Figure 2). The first mixing zone contained 12 kneading elements with angles of 30°, 60°, and 90°; the second mixing zone contained 6 kneading elements with an angle of 60°; and the third mixing zone consisted of 8 kneading elements with angles of 60° followed by 90°. Extrusion at 115°C of a plain ARP-ADP PM without a polymer resulted in processing torque exceeding the instrument maximum limit. After the initial extrusion trials, a modified screw configuration (without the third mixing zone and all screws replaced with the conveying elements) was utilized.

However, extrusion with the modified screw configuration could not facilitate the processing of plain cocrystal components due to high processing torque values. To facilitate the extrusion with the standard screw configuration, 5% SOL was incorporated into the ARP-ADP blend, which enabled the HME process to complete with processing torque values within the instrument's normal limit. Therefore, processing of a PM with an equimolar ratio of ARP and ADP was feasible in the presence of 5% SOL which indicated its applicability in producing pharmaceutical cocrystals. The presence of SOL, which is a low glass transition temperature polymeric carrier, improves processability and facilitates the interaction between ARP and ADP to form cocrystals during extrusion. These results indicate the selection of an appropriate polymer with the desired thermal properties to develop pharmaceutical cocrystals. They are in accordance with previous reports using SOL as a polymeric excipient for cocrystals of theophylline and ibuprofen with nicotinamide by the HME process.[32,33] Further, effects of screw speed and temperature profile on the formation of cocrystals were reported in Table 1, while other HME parameters, such as feed rate (0.4 g/min) and standard screw configuration, were held constant.

Effect of HME processing parameters on cocrystal formation

Temperature—The temperature of the barrel during extrusion is very important, as it can impact the residence time of components in the extruder and the formation of cocrystals. Extrusion at low temperature increases the processing torque and reduces the mass transfer and contact of cocrystal components, which results in incomplete cocrystallization. In order to obtain good quality cocrystals in the HME process, the processing temperature should be below the melting point of the cocrystals.[34] Daurio *et al*[31] studied the effect of extruder barrel temperature on the formation of AMG 519-sorbic acid cocrystals. The results indicate complete conversion of cocrystals when the barrel temperature was less than the melting points of the individual components. The findings also conclude that increase in the barrel temperature close to the cocrystal formation temperature led to efficient cocrystallization. Therefore, in the present study extrusion was carried out at 100°C, 115°C, and 125°C. At 100°C, the formation of cocrystals was incomplete, indicating that the components were unreacted and the mass transfer between components could not take place. Extrusion at 125°C resulted in the melting of the physical blend within the barrel. However, at 115°C and in the presence of SOL, uniform mixing of ARP and ADP was observed. In order to facilitate contact and mass transfer between ARP and ADP, the processing temperature was set to 115°C.

Screw speed—Screw speed is directly related to the residence time and flow of the blend within the barrel, which impacts the formation of cocrystals. To examine the effect of screw speed on cocrystal formation, the temperature was kept constant at 115°C while the screw speed was varied between 25 and 75 rpm at intervals of 25 rpm. No change in the melting point of the cocrystals was observed in DSC thermograms at different screw speeds, which confirmed that cocrystal formation was complete at all screw speeds studied and indicated that each screw speed provided sufficient residence time in the barrel for components to form cocrystals. Thus, no impact from screw speed on cocrystal formation was observed, which is in line with a similar observation reported by Karimi-Jafari et al[33], studied the effect of screw speeds on the cocrystallization. In another study, Daurio *et al*[30] investigated

the effect of screw speed on the residence time and conversion of caffeine-oxalic acid cocrystals. The results indicate that though cocrystal formation was observed at all screw speeds, cocrystals processed at higher screw speed showed the presence of residual caffeine, indicating incomplete cocrystal conversion.

From the DSC results, it was observed that cocrystal formation was complete regardless of the selected screw speeds. Thus, the processing of ARP-ADP cocrystals was optimal with 5% SOL in standard screw configuration at a temperature of 115°C and a screw speed of 50 rpm, and the extrudates with these process parameters were evaluated by solid state characterization and *in vitro* dissolution studies.

Thermal analysis—DSC studies were carried out to determine the thermal behavior of ARP, ADP, PM of ARP-ADP and the cocrystals. The thermograms of pure ARP, ADP, PM and the cocrystals are shown in Figure 3. Pure ARP exhibited an endothermic peak at 139°C due to its melting behavior[24,27] and ADP showed an endothermic peak at 155°C, indicating the crystalline nature of the cocrystal components. From the DSC thermogram of PM, it was observed that the PM of ARP and ADP forms a eutectic i.e., melting at a lower temperature than that of the two cocrystal components. This could be attributed to the suppression of ARP melting point in the presence of ADP. Similar observations were reported for itraconazole–succinic acid cocrystals, where the PM has shown melting endotherm at 151°C, which is less than the melting temperature of itraconazole (169°C) and succinic acid (191°C).[35] The PM of ARP and ADP produces two endothermic peaks in the DSC thermogram (Figure 3 H). The first endothermic peak corresponding to the eutectics and the second endothermic peak corresponding to cocrystal melting temperature. The melting temperature of ARP and ADP in the PM was close to the cocrystal melting temperature, which led to the overlapping of thermal effects. These type of thermal effects overlap noticed while analyzing the PM with melting temperature difference between cocrystal components less than 50°C.[36] Cocrystals processed by HME at 100°C showed a blunt endothermic peak at 128°C, suggesting unreacted components of the cocrystals and the cocrystals processed at 115°C showed a sharp endothermic peak at 128°C, suggesting the complete formation of cocrystals. Furthermore, DSC thermograms of cocrystals processed at 115°C, with varied screw speeds of 25, 50, and 75 rpm, showed a sharp endothermic peak at 128°C, confirming the formation of cocrystals without effects from the screw speed. The formation of cocrystals in the extruder is due to the eutectic behavior between cocrystal components.[8] The processing temperature above the eutectic melting temperature is likely to be responsible for efficient cocrystalization in the extruder. From the previous literature, it was evident that cocrystals can be formed from the eutectic melt.[8] The possible mechanisms responsible for mechano-chemical reaction between cocrystal components are the existence of an intermediate phase which can be either eutectic/vapor/ amorphous state.[31]

The melting point depression or enhancement of cocrystals depends on the cocrystallization method. As reported by Schultheiss et al,[37] 59% of cocrystal systems exhibited a melting point between those of drug and the coformer, 39% had a melting point lower than either the drug or the coformer, 4% had similar melting points as the drug or coformer, and 6% had a melting point higher than those of the drug and coformer. The cocrystal formulations exhibited lower heat of fusion or enthalpy (76.2 and 74.3 J/g respectively for liquid-assisted

grinding and HME cocrystals) than the pure ARP (91.3 J/g) and ADP (140.6 J/g). The lower enthalpy value of the cocrystals could be attributed to increased interaction and miscibility between ARP and ADP, which might have led to reduced intensity in the endothermic peaks of cocrystals compared to the pure ARP and ADP. These observations were in accordance with the previous reports[38].

HSM analysis—HSM studies were conducted to examine the thermal transitions and melting of ARP and cocrystals at different rates of heating.[4] HSM images of pure ARP and cocrystals are shown in Figure 4. DSC thermograms supported the HSM findings. No thermal event was observed until melting temperatures of 139°C and 128°C for ARP and cocrystals, respectively. The cocrystals appeared as crystalline material at room temperature, and undissolved cocrystals were observed at temperatures below 128°C. During the progression of thermal events, cocrystals began to dissolve at 128°C, and complete melting was observed above 130°C. Similar results were observed for pure ARP, as shown in the HSM images, and complete melting was observed above 140°C. These findings suggest that ARP and ADP interacted with each other during thermal processing.

FTIR and chemical imaging analysis—Figure 5 illustrates the FTIR spectra of ARP, ADP, PM of ARP-ADP and the corresponding cocrystals. ARP showed characteristic bands of C=O stretching vibrations at 1673 cm^{-1} and N-H bending vibrations appeared at 1627 cm^{-1}. Aromatic ring C=C–C stretching vibrations located at 1594 cm^{-1}, aliphatic C–H stretching vibrations arises at 2945 cm^{-1}, and C-H bending vibration appears at 1444 and 1375 cm^{-1}.[5,39,40] The FTIR spectra of ADP showed C=O stretching vibrations at 1681 cm^{-1} and O-H stretching bands at 2950 cm^{-1}.[41,42] The PM of ARP-ADP shows frequency bands specific to the individual components with the change in intensity of the peaks compared to the individual starting components. The FTIR spectra of cocrystals showed the ARP characteristic bands corresponding to the C=O stretching vibration shifted from 1673 to 1679 cm^{-1}. Also, the ARP characteristic bands 1444 and 1376 cm^{-1} shifted in the cocrystal spectrum to 1451 and 1387 cm^{-1}, respectively. In the same way, a decrease in O-H stretching frequencies of the adipic acid from 2950 cm^{-1} to 2938 cm^{-1} was observed in the cocrystals. The shift in the C=O stretching of ARP and O-H stretching band of ADP in the cocrystals attributed to the formation of a hydrogen bond between the cocrystal components.[41] Moreover, for the cocrystals, a new peak appeared at 1720 cm^{-1}.

Nanubolu *et al*[27] investigated the cocrystals of ARP with mutihydroxy benzene coformers. They reported that characteristic amide C=O peak in the ARP shifted in the cocrystals from 1679 cm^{-1} to 1673, 1662, 1653, 1652 and 1652 cm^{-1} respectively for cocrystals prepared with catechol, hydroquinone, resorcinol, pyrogallol and phloroglucinol coformers. These shifts in the frequency are attributed to the participation of the carbonyl group (C=O) in the hydrogen bonding with the mutihydroxy benzene coformers. Further, their findings also state that larger C=O shifts are indicative of stronger hydrogen bonding in the cocrystals.

In the ARP-ADP cocrystals, a shift in the frequencies of the functional groups compared to that of ARP and ADP indicate the presence of hydrogen bond formation between ARP and ADP. These findings in the FTIR spectra could be due to the noncovalent interaction

between cocrystal components and results in the formation of cocrystals. There was no change in the band position or intensity of cocrystals processed at different screw speeds.

Figure. 6 shows chemical imaging of ARP-ADP cocrystals. Analysis was performed to determine the distribution of cocrystals and identify the cocrystals from their components. Attenuated total reflectance (ATR), which is direct contact with the sample surface, was used to investigate the distribution of cocrystals at different positions of the extrudates. As shown by the bench top FTIR spectrum, chemical imaging of cocrystals also exhibited peaks at 1720 cm^{-1} and 1679 cm^{-1}. The obtained wavenumber position was uniform throughout the different positions of the captured image, indicating the uniform distribution of cocrystals in the obtained extrudate powder. These findings were in accordance with the previous literature.[43]

PXRD analysis—The powder X-ray diffraction patterns of ARP, ADP, PM and the cocrystals at different screw speeds are shown in Figure 7. The ARP diffractogram shows reflections at 2θ values of 16.46°, 19.36°, 20.22°, 21.82°, and 24.68°[40,44]; the diffractogram of ADP showed diffraction peaks at 2θ values of 13.14°, 21.6°, 26.18°, 31.32°, and 42.16°[42] and these diffraction peaks are attributed to the crystalline nature of the starting components. The diffractogram of PM showed reflections corresponding to the individual components of ARP, ADP with no change in the position of 2θ values. The cocrystals showed characteristic peaks at 2θ values of 17.32°, 18.46°, 22.3°, and 25.12°, which were not present in either ARP or ADP and were attributed to interactions between the two components resulting in new crystalline material. PXRD is a signature and reliable technique in the characterization and differentiation of cocrystals and eutectics from their parent components.[45] Unlike eutectics where a diffraction pattern represents the combination of individual parent components, cocrystals are characterized by the presence of distinct peaks due to formation of new crystalline material. Hence, the presence of distinct peaks in the PXRD pattern of ARP-ADP cocrystals rules out the formation of eutectics.[46] Diffraction peaks of cocrystals processed at different screw speeds showed no difference in the intensity and 2θ values, indicates the formation of cocrystals was complete. These results were in line with the previous literature. Studies from Daurio *et al*[30] concludes that the extent of cocrystal conversion moderately depends on the screw speed of the extruder and significantly depends on the barrel temperature in the extruder.

Characterization of ARP-ADP cocrystals by solution-phase NMR—ARP, ADP, and the cocrystals were characterized by ^{1}H-NMR and ^{13}C NMR spectral techniques. The ^{1}H NMR spectrum of ADP clearly showed an equivalent free hydroxyl group peak at δ 12.0 ppm. In addition, ADP also exhibited corresponding NMR signals for the α & β carbon protons of the carboxyl functional group at δ 2.20 ppm & 1.50 ppm, respectively. The ^{13}C NMR spectrum of ADP showed a carbonyl peak at δ 175.0 ppm, whereas the α & β carbon signals appeared at δ 34.0 ppm & δ 24.0 ppm, respectively. The ^{1}H NMR spectrum of ARP showed a free amide proton peak at δ 10.0 ppm. The six aromatic protons (three protons from the phenyl ring and three from the pharmacophore) appeared in the range of δ 6.30 to 7.50 ppm. The eight aliphatic protons of the piperazine ring, as well as the butyl chain and two aliphatic protons of the pharmacophore, appeared in the range of δ 1.50 to 4.00 ppm.

The ^{13}C NMR spectrum of ARP showed a carbonyl peak at δ 170.0 ppm, whereas the aromatic carbons appeared in the range of δ 100.0 to 160.0 ppm, and all other aliphatic carbons showed corresponding signals in the upfield region (*i.e.*, less than 70.0 ppm). The ^{1}H NMR spectrum of the cocrystals clearly showed the presence of proton signals of ARP and ADP, except for the presence of a free hydroxyl peak of ADP at δ 12.0 ppm (Figure. 8). The ^{13}C NMR spectrum of the cocrystals showed carbonyl peaks in ARP and ADP at δ 170.0 & 175.0 ppm, respectively, and other carbon signals in cocrystals were identical with the carbon signals of the individual ^{13}C NMR spectra of ARP and ADP (Figure.9). Therefore, these spectra suggest that non-covalent interaction between ARP and ADP and confirms the formation of ARP-ADP cocrystals.

SEM analysis—The SEM images (Figure. 10) of ARP show broken, irregularly shaped crystals, and those of ADP show smooth surface crystals. The cocrystals were found to be clustered with smooth surfaces, indicating that the cocrystals processed by HME were packed together, which could be attributed to efficient mixing within the barrel. These differences in the size and shape of cocrystals indicate molecular interaction between cocrystal components. Thus, the morphology of the cocrystals was entirely different from those of ARP and ADP, which indicated the formation of new crystalline material. The morphology of newly formed cocrystals could influence physicochemical and mechanochemical parameters, such as solubility, dissolution, flowability, and compressibility characteristics, which could be advantageous to the development of pharmaceutical solid dosage forms.

Solubility and *in-vitro* dissolution studies—The solubility of ARP and cocrystals was found to be 2.8 ± 0.93, 22.6 ± 1.9 μg/mL respectively. Cocrystals improved the solubility by 8.1-fold compared to pure ARP. *In-vitro* dissolution studies were conducted to determine the performance of HME-processed cocrystals compared with pure ARP and ARP with 5% SOL. ARP showed solubility that varied inversely with pH;[5] hence, a higher pH dissolution medium has better dissolution rate discrimination compared with a lower pH medium.[20] Therefore, *in vitro* drug release of cocrystals was performed in deionized (DI) water as a discriminating dissolution medium and compared with pure ARP and ARP with 5% SOL.[28] As shown in Figure 11, the dissolution rate of pure ARP and ARP-5% SOL was 2.10 and 2.95 μg/mL respectively at 2 h time interval. In contrast, cocrystals showed a dissolution rate of 14.80 μg/mL at the end of 2 h. The maximum concentration of ARP from the cocrystals was 14.80 μg/mL, which is approximately 7.0 and 5.1-fold greater than that of pure ARP and ARP-5% SOL respectively. The dissolution profile of ARP with 5% SOL resulted in increased dissolution rate (1.4 fold) compared to the pure ARP. The presence of SOL plays an important role in accelerating the dissolution rate of cocrystals due to its hydrophilic and solubilizing nature.[47] There is no significant difference in the dissolution profiles of cocrystals processed at different screw speeds. This faster dissolution rate of cocrystals may be attributed to intermolecular interaction between ARP and ADP in the formation of cocrystals. The drug content of the cocrystal formulations was in the range of 95.5% to 98.5%, which is within acceptable limits.

Flow properties and true density—Different flow parameters, such as bulk density, tapped density, CI, and HR, were determined to assess the flowability of pure ARP and the cocrystals. The results of these determinations are presented in Table 2. The CI and HR of pure ARP were found to be 41 ± 5.02 and 1.69 ± 0.19, respectively. The CI and HR of the cocrystals were 24± 2.02 and 1.31± 0.17, respectively. A CI >38 and HR >1.60 are indicative of very, very poor flow characteristics, whereas a CI between 21 and 25 and HR between 1.26 and 1.34 is considered passable flow.[48] These results suggest that the HME-processed cocrystals have better flow properties compared with pure ARP. This improved flow may be due to the relatively good flow properties of ADP and SOL in the cocrystals.

The true densities of ARP and the cocrystals were 1.318 ± 0.0009 g/cm^3 and 1.391 ± 0.0003 g/cm^3, respectively. The true density values show that the cocrystals are relatively denser than pure ARP. An increase in particle density and a loss of voids can occur during hot melt extrusion due to heat and shear stress.[49] Also, increase in density and improved flow properties of cocrystals could be due to the densification of material when processed by HME. This variation in the true density values of ARP and the cocrystals suggests that the cocrystals are more compressible than the pure ARP.

CONCLUSION

In the present work, HME was successfully employed to produce ARP-ADP cocrystals. The low Tg matrix polymer (SOL) played an important role in the extrusion by facilitating the processability of the ARP-ADP PM. The extrusion temperature was observed to be a critical parameter influencing the formation of cocrystals. Further, cocrystal formation was verified by DSC, FTIR, PXRD, NMR studies, and the FTIR, NMR results confirmed non-covalent interaction between ARP and ADP. Cocrystals produced by HME technique improved the solubility (8-fold) and dissolution rate (7-fold) compared with the pure ARP. *In-vitro* solubility and dissolution advantages of cocrystals need to be confirmed by performing the *in-vivo* studies. The HME process utilized for cocrystals production can be scaled up by volumetric scale-up approach with stability studies in the future. Thus, a scalable and industrially feasible continuous HME manufacturing process may be an alternative to conventional methods for the production of pharmaceutical cocrystals.

ACKNOWLEDGMENTS

This project was supported by grant number P30GM122733–01A1. We would like to thank Indika Chandrasiri, Mahesh Loku Yaddehige (Department of Chemistry and Biochemistry, University of Mississippi) and Dr. N. Sridhar Goud (National Institute of Mental Health & Neuro Sciences, Bengaluru, Karnataka, India) for their assistance in NMR results interpretation.

ABBREVIATIONS

API	active pharmaceutical ingredient
ADP	adipic acid
ARP	Aripiprazole
CI	Carr index

DSC	differential scanning calorimetry
FDA	Food and Drug Administration
FTIR	Fourier transform infrared spectroscopy
HR	Hausner ratio
HME	Hot melt extrusion
HSM	hot-stage microscopy
NMR	nuclear magnetic resonance spectroscopy
PM	Physical mixture
PXRD	powder X-ray diffraction
SEM	scanning electron microscopy

REFERENCES

(1). Liu X; Zhou L; Zhang F Reactive Melt Extrusion To Improve the Dissolution Performance and Physical Stability of Naproxen Amorphous Solid Dispersions. Mol. Pharmaceutics 2017, 14, 658–673.

(2). Formulating Poorly Water Soluble Drugs; III, R. O. W., Watts AB, Miller DA, Eds.; AAPS Advances in the Pharmaceutical Sciences Series; Springer-Verlag: New York, 2012.

(3). Leuner C; Dressman J Improving Drug Solubility for Oral Delivery Using Solid Dispersions. Eur. J. Pharm. Biopharm 2000, 50, 47–60. [PubMed: 10840192]

(4). Moradiya HG; Islam MT; Halsey S; Maniruzzaman M; Chowdhry BZ; Snowden MJ; Douroumis D Continuous Cocrystallisation of Carbamazepine and Trans-Cinnamic Acid via Melt Extrusion Processing. CrystEngComm 2014, 16, 3573–3583.

(5). Mihajlovic T; Kachrimanis K; Graovac A; Djuric Z; Ibric S Improvement of Aripiprazole Solubility by Complexation with (2-Hydroxy)Propyl-β-Cyclodextrin Using Spray Drying Technique. AAPS PharmSciTech 2012, 13, 623–631. [PubMed: 22535520]

(6). Karri V; Butreddy A; Dudhipala N Fabrication of Efavirenz Freeze Dried Nanocrystals: Formulation, Physicochemical Characterization, In Vitro and Ex Vivo Evaluation. Adv. Sci., Eng. Med 2015, 7, 385–392.

(7). B, A.; D, N.; Veerabrahma K Development of Olmesartan Medoxomil Lipid-Based Nanoparticles and Nanosuspension: Preparation, Characterization and Comparative Pharmacokinetic Evaluation. Artif. Cells. Nanomed., Biotechnol 2018, 46, 126–137. [PubMed: 28290712]

(8). Lu E; Rodríguez-Hornedo N; Suryanarayanan R A Rapid Thermal Method for Cocrystal Screening. CrystEngComm 2008, 10, 665–668.

(9). Kelly AL; Gough T; Dhumal RS; Halsey SA; Paradkar A Monitoring Ibuprofen-Nicotinamide Cocrystal Formation during Solvent Free Continuous Cocrystallization (SFCC) Using near Infrared Spectroscopy as a PAT Tool. Int. J. Pharm 2012, 426, 15–20. [PubMed: 22274588]

(10). Shaikh R; Walker GM; Croker DM Continuous, Simultaneous Cocrystallization and Formulation of Theophylline and 4-Aminobenzoic Acid Pharmaceutical Cocrystals Using Twin Screw Melt Granulation. Eur. J. Pharm. Sci 2019, 137, 104981. [PubMed: 31295548]

(11). Trask AV; Jones W Crystal Engineering of Organic Cocrystals by the Solid-State Grinding Approach. Org. Solid-State React 2015, 41–70.

(12). Rothenberg G; Downie AP; Raston CL; Scott JL Understanding Solid/Solid Organic Reactions. J. Am. Chem. Soc 2001, 123, 8701–8708. [PubMed: 11535074]

(13). Chadwick K; Davey R; Cross W How Does Grinding Produce Co-Crystals? Insights from the Case of Benzophenone and Diphenylamine. CrystEngComm 2007, 9, 732–734.

(14). Hsi KH-Y; Chadwick K; Fried A; Kenny M; Myerson AS Separation of Impurities from Solution by Selective Co-Crystal Formation. CrystEngComm 2012, 14, 2386–2388.

(15). Aher S; Dhumal R; Mahadik K; Paradkar A; York P Ultrasound Assisted Cocrystallization from Solution (USSC) Containing a Non-Congruently Soluble Cocrystal Component Pair: Caffeine/Maleic Acid. Eur. J. Pharm. Sci 2010, 41, 597–602. [PubMed: 20801215]

(16). Padrela L; Rodrigues MA; Velaga SP; Matos HA; de Azevedo EG Formation of Indomethacin–Saccharin Cocrystals Using Supercritical Fluid Technology. Eur. J. Pharm. Sci 2009, 38, 9–17. [PubMed: 19477273]

(17). Aakeröy CB; Forbes S; Desper J The Effect of Water Molecules in Stabilizing Co-Crystals of Active Pharmaceutical Ingredients. CrystEngComm 2012, 14, 2435–2443.

(18). Buanz ABM; Telford R; Scowen IJ; Gaisford S Rapid Preparation of Pharmaceutical Co-Crystals with Thermal Ink-Jet Printing. CrystEngComm 2013, 15, 1031–1035.

(19). Fernandes GJ; Rathnanand M; Kulkarni V Mechanochemical Synthesis of Carvedilol Cocrystals Utilizing Hot Melt Extrusion Technology. J. Pharm. Sci. Innovation 2019, 14, 373–381.

(20). Dhumal RS; Kelly AL; York P; Coates PD; Paradkar A Cocrystalization and Simultaneous Agglomeration Using Hot Melt Extrusion. Pharm. Res 2010, 27, 2725–2733. [PubMed: 20872053]

(21). Chavan RB; Thipparaboina R; Yadav B; Shastri NR Continuous Manufacturing of Co-Crystals: Challenges and Prospects. Drug Delivery Transl. Res 2018, 1726–1739.

(22). Medina C; Daurio D; Nagapudi K; Alvarez-Nunez F Manufacture of Pharmaceutical Co-crystals Using Twin Screw Extrusion: A Solvent-less and Scalable Process. J. Pharm. Sci 2010, 1693–1696. [PubMed: 19774652]

(23). Xu Y; Liu X; Lian R; Zheng S; Yin Z; Lu Y; Wu W Enhanced Dissolution and Oral Bioavailability of Aripiprazole Nanosuspensions Prepared by Nanoprecipitation/Homogenization Based on Acid–Base Neutralization. Int. J. Pharm 2012, 438, 287–295. [PubMed: 22989976]

(24). McFall H; Sarabu S; Shankar V; Bandari S; Murthy SN; Kolter K; Langley N; Kim DW; Repka MA Formulation of Aripiprazole-Loaded PH-Modulated Solid Dispersions via Hot-Melt Extrusion Technology: In Vitro and in Vivo Studies. Int. J. Pharm 2019, 302–311. [PubMed: 30395959]

(25). Wang J-R; Ye C; Zhu B; Zhou C; Mei X Pharmaceutical Cocrystals of the Anti-Tuberculosis Drug Pyrazinamide with Dicarboxylic and Tricarboxylic Acids. CrystEngComm 2014, 17, 747–752.

(26). Sarceviča I; Kons A; Orola L Isoniazid Cocrystallisation with Dicarboxylic Acids: Vapochemical, Mechanochemical and Thermal Methods. CrystEngComm 2016, 18, 1625–1635.

(27). Nanubolu JB; Ravikumar K Correlating the Melting Point Alteration with the Supramolecular Structure in Aripiprazole Drug Cocrystals. CrystEngComm 2016, 18, 1024–1038.

(28). Cho M-Y; Kim P; Kim G-Y; Lee J-Y; Song K-H; Lee M-J; Yoon W; Yun H; Choi GJ Preparation and Characterization of Aripiprazole Cocrystals with Coformers of Multihydroxybenzene Compounds. Cryst. Growth Des 2017, 17, 6641–6652.

(29). Paul S; Chang S-Y; Dun J; Sun W-J; Wang K; Tajarobi P; Boissier C; Sun CC Comparative Analyses of Flow and Compaction Properties of Diverse Mannitol and Lactose Grades. Int. J. Pharm 2018, 546, 39–49. [PubMed: 29705102]

(30). Daurio D; Medina C; Saw R; Nagapudi K; Alvarez-Núñez F Application of Twin Screw Extrusion in the Manufacture of Cocrystals, Part I: Four Case Studies. Pharmaceutics 2011, 3, 582–600. [PubMed: 24310598]

(31). Daurio D; Nagapudi K; Li L; Quan P; Nunez F-A Application of Twin Screw Extrusion to the Manufacture of Cocrystals: Scale-up of AMG 517–Sorbic Acid Cocrystal Production. Faraday Discuss 2014, 170, 235–249. [PubMed: 25406487]

(32). Gajda M; Nartowski KP; Pluta J; Karolewicz B Tuning the Cocrystal Yield in Matrix-Assisted Cocrystallisation via Hot Melt Extrusion: A Case of Theophylline-Nicotinamide Cocrystal. Int. J. Pharm 2019, 569, 118579. [PubMed: 31362095]

(33). Karimi-Jafari M; Ziaee A; Iqbal J; O'Reilly E; Croker D; Walker G Impact of Polymeric Excipient on Cocrystal Formation via Hot-Melt Extrusion and Subsequent Downstream Processing. Int. J. Pharm 2019, 566, 745–755. [PubMed: 31212053]

(34). Gajda M; Nartowski KP; Pluta J; Karolewicz B The Role of the Polymer Matrix in Solvent-Free Hot Melt Extrusion Continuous Process for Mechanochemical Synthesis of Pharmaceutical Cocrystal. Eur. J. Pharm. Biopharm 2018, 131, 48–59. [PubMed: 30205892]

(35). Ober CA; Gupta RB Formation of Itraconazole–Succinic Acid Cocrystals by Gas Antisolvent Cocrystallization. AAPS PharmSciTech 2012, 13, 1396–1406. [PubMed: 23054991]

(36). Manin AN; Voronin AP; Drozd KV; Manin NG; Bauer-Brandl A; Perlovich GL Cocrystal Screening of Hydroxybenzamides with Benzoic Acid Derivatives: A Comparative Study of Thermal and Solution-Based Methods. Eur. J. Pharm. Sci 2014, 65, 56–64. [PubMed: 25218047]

(37). Schultheiss N; Newman A Pharmaceutical Cocrystals and Their Physicochemical Properties. Cryst. Growth Des 2009, 9, 2950–2967.

(38). Al-Kazemi R; Al-Basarah Y; Nada A Dissolution Enhancement of Atorvastatin Calcium by Cocrystallization. Adv. Pharm. Bull 2019, 9, 559–570. [PubMed: 31857959]

(39). Casey AB; Canal CE Classics in Chemical Neuroscience: Aripiprazole. ACS Chem. Neurosci 2017, 8, 1135–1146. [PubMed: 28368577]

(40). Braun DE; Gelbrich T; Kahlenberg V; Tessadri R; Wieser J; Griesser UJ Stability of Solvates and Packing Systematics of Nine Crystal Forms of the Antipsychotic Drug Aripiprazole. Cryst. Growth Des 2009, 9, 1054–1065.

(41). Borodi G; Turza A; Onija O; Bende A Succinic, Fumaric, Adipic and Oxalic Acid Cocrystals of Promethazine Hydrochloride. Acta Crystallogr., Sect. C: Struct. Chem 2019, 75, 107–119. [PubMed: 30720448]

(42). Espinosa-Lara JC; Guzman-Villanueva D; Arenas-García JI; Herrera-Ruiz D; Rivera-Islas J; Román-Bravo P; Morales-Rojas H; Höpfl H Cocrystals of Active Pharmaceutical Ingredients—Praziquantel in Combination with Oxalic, Malonic, Succinic, Maleic, Fumaric, Glutaric, Adipic, And Pimelic Acids. Cryst. Growth Des 2013, 13, 169–185.

(43). Vo AQ; Feng X; Morott JT; Pimparade MB; Tiwari RV; Zhang F; Repka MA A Novel Floating Controlled Release Drug Delivery System Prepared by Hot-Melt Extrusion. Eur. J. Pharm. Biopharm 2016, 98, 108–121. [PubMed: 26643801]

(44). Tan X; Zhong Y; He L; Zhang Y; Jing G; Li S; Wang J; He H; Tang X Morphological and Crystalline Transitions in Monohydrous and Anhydrous Aripiprazole for a Long-Acting Injectable Suspension. AAPS PharmSciTech 2017, 18, 1270–1276. [PubMed: 27480439]

(45). Cherukuvada S; Nangia A Eutectics as Improved Pharmaceutical Materials: Design, Properties and Characterization. Chem. Commun 2013, 50, 906–923.

(46). Jagia M; Daptardar R; Patel K; Bansal AK; Patel S Role of Structure, Microenvironmental PH, and Speciation To Understand the Formation and Properties of Febuxostat Eutectics. Mol. Pharm 2019, 16, 4610–4620. [PubMed: 31573811]

(47). Boksa K; Otte A; Pinal R Matrix-Assisted Cocrystallization (MAC) Simultaneous Production and Formulation of Pharmaceutical Cocrystals by Hot-Melt Extrusion. J. Pharm. Sci 2014, 103, 2904–2910. [PubMed: 24807421]

(48). Shah RB; Tawakkul MA; Khan MA Comparative Evaluation of Flow for Pharmaceutical Powders and Granules. AAPS PharmSciTech 2008, 9, 250–258. [PubMed: 18446489]

(49). Agrawal A; Dudhedia M; Deng W; Shepard K; Zhong L; Povilaitis E; Zimny E Development of Tablet Formulation of Amorphous Solid Dispersions Prepared by Hot Melt Extrusion Using Quality by Design Approach. AAPS PharmSciTech 2016, 17, 214–232. [PubMed: 26757898]

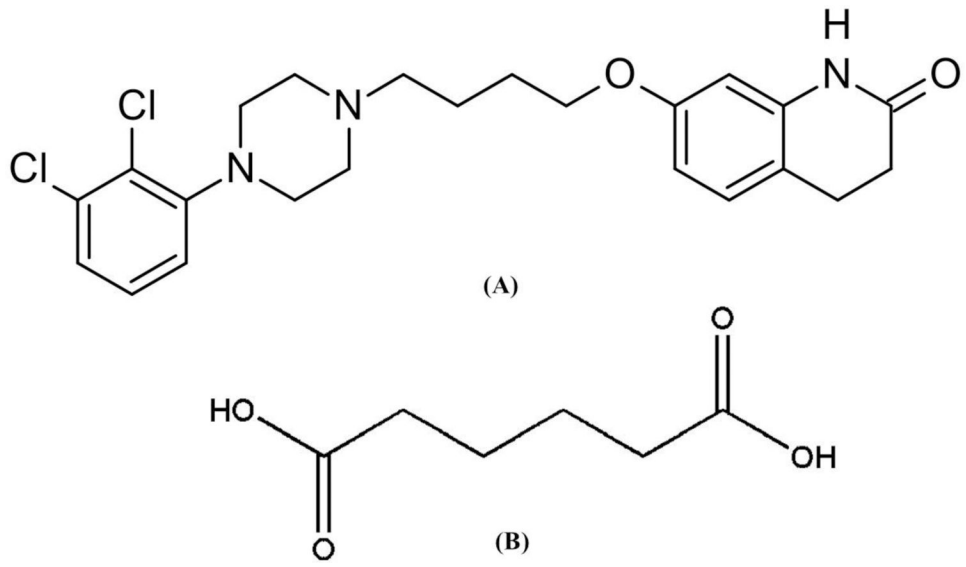

Figure 1.
Chemical structures of (A) aripiprazole, (B) adipic acid.

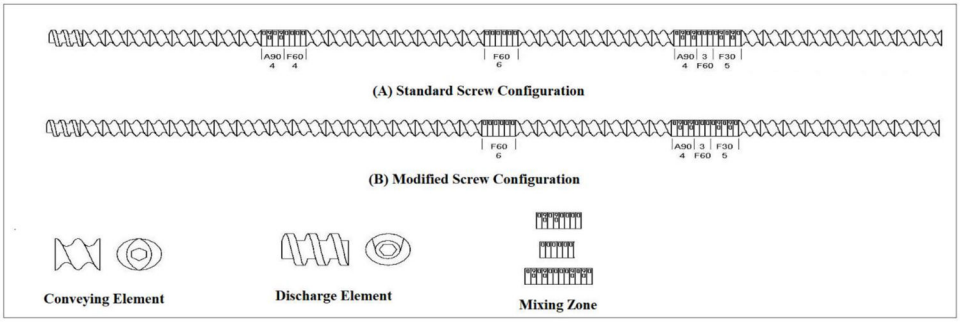

Figure 2.
Schematic diagram of screw configuration used in HME.

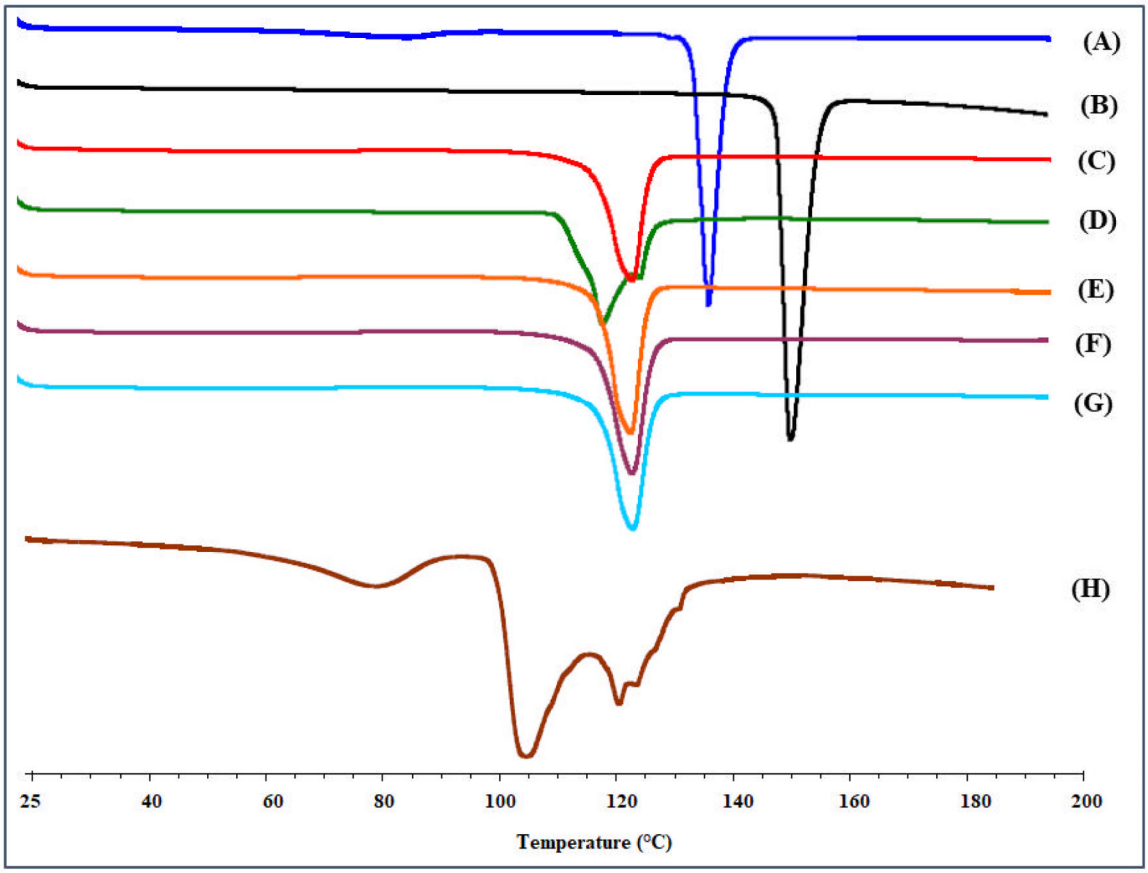

Figure 3.

DSC thermograms of a) pure ARP, b) bulk ADP, c) cocrystals prepared by liquid grinding method, and d) cocrystals processed at 100°C, 50 rpm, e) at 115°C, 25 rpm, f) at 115°C, 50 rpm, g) at 115°C, 75 rpm and h) PM of ARP-ADP.

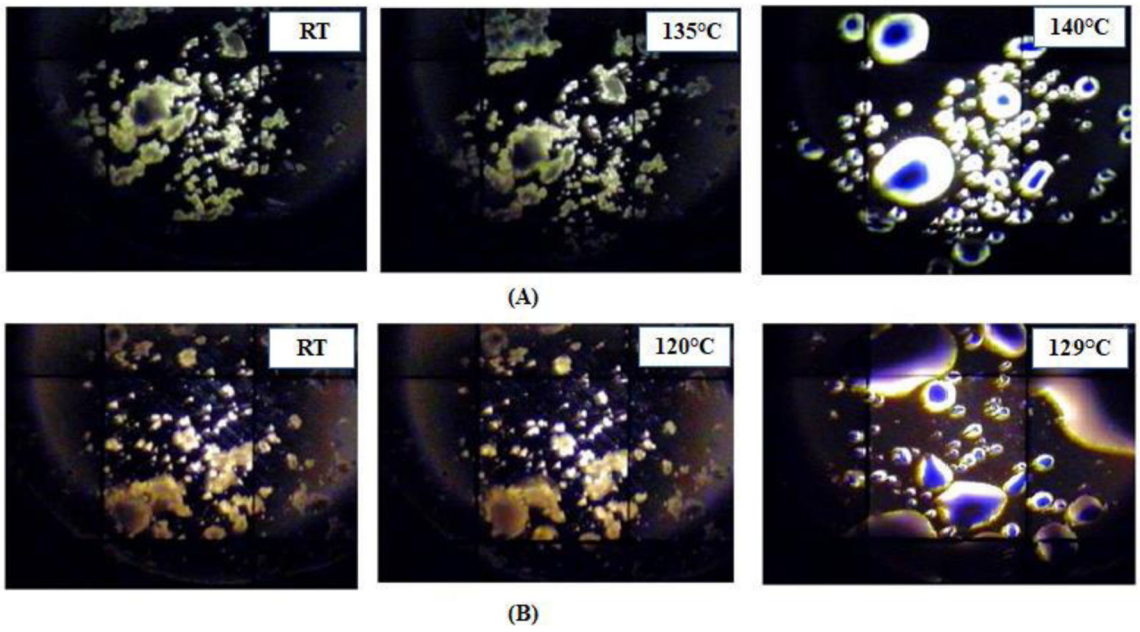

Figure 4.
HSM images of a) ARP, b) ARP-ADP cocrystals.

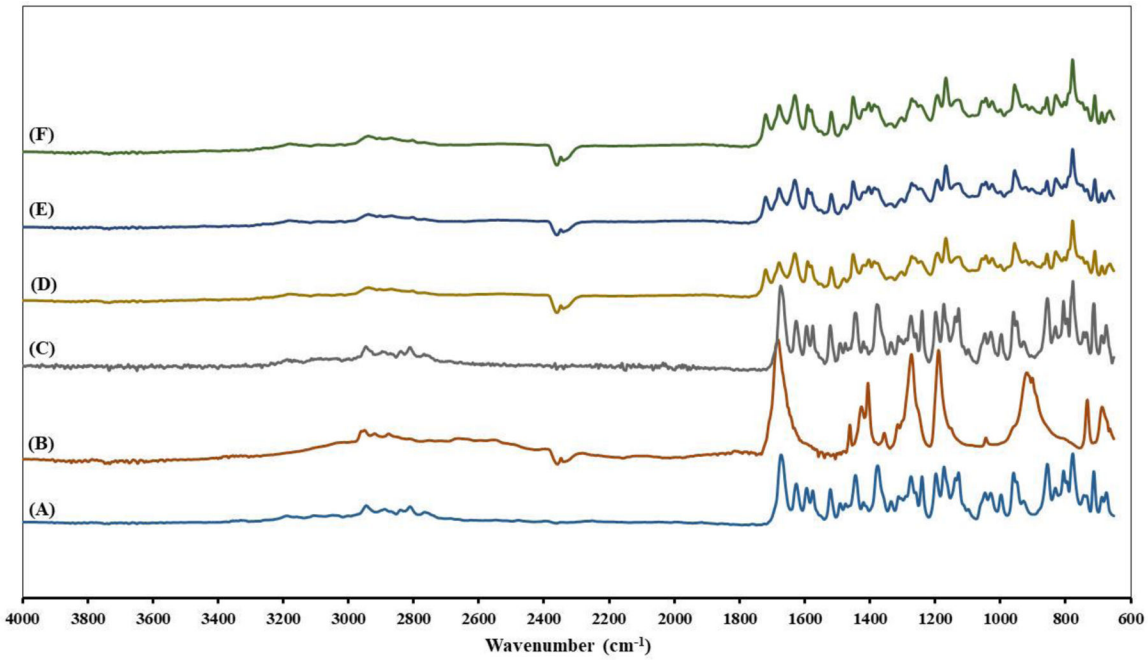

Figure 5.
FTIR spectra of a) ARP, b) ADP, c) PM of ARP-ADP, and d) ARP-ADP cocrystals at screw speed 25 rpm, e) 50 rpm, and f) 75 rpm.

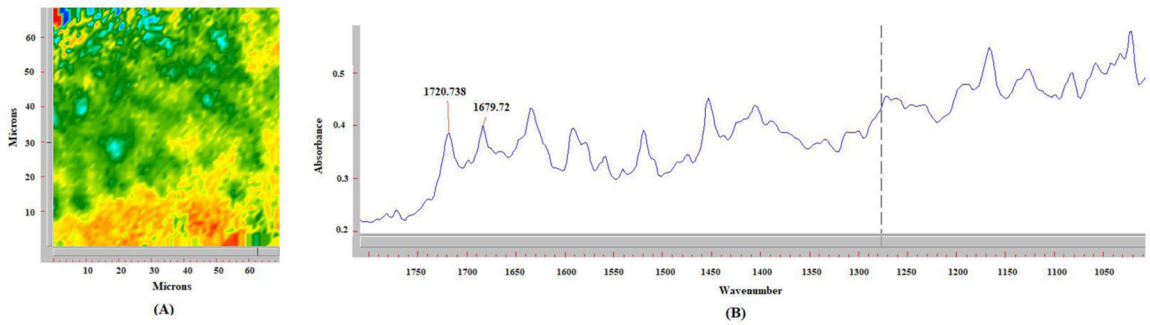

Figure 6.

A) Chemical image of ARP-ADP cocrystals with Ge ATR at 1.1 μm spatial resolution, B) FTIR spectra of cocrystals specific to chemical imaging.

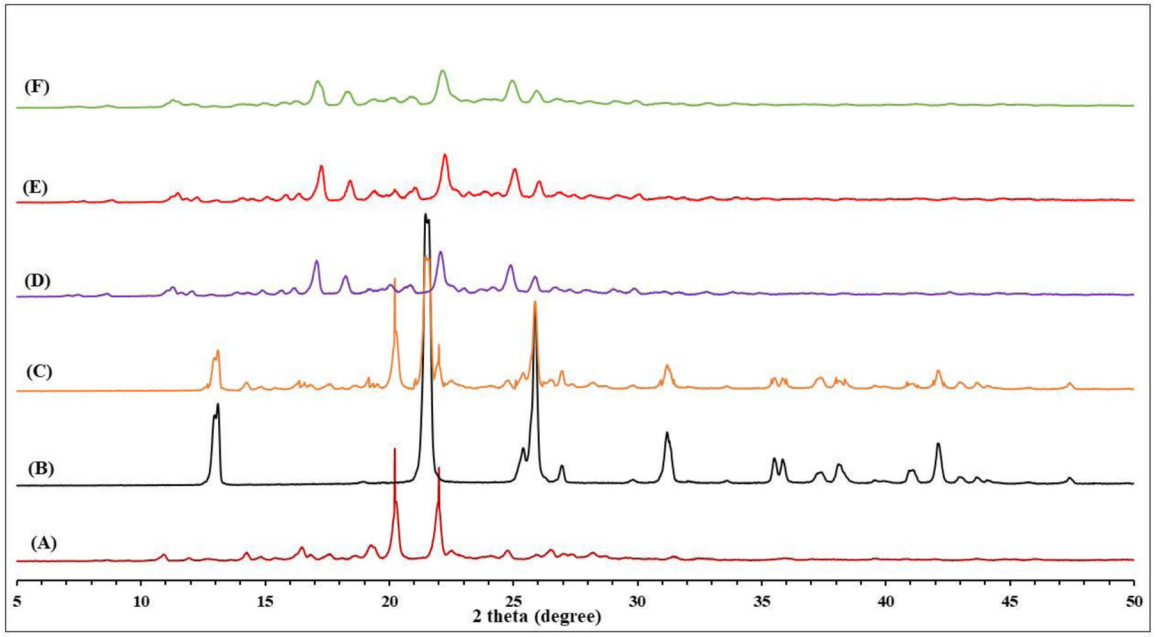

Figure 7.

PXRD diffractograms of a) ARP, b) ADP, c) PM of ARP-ADP and d) ARP-ADP cocrystals at screw speed 25 rpm, e) 50 rpm, and f) 75 rpm.

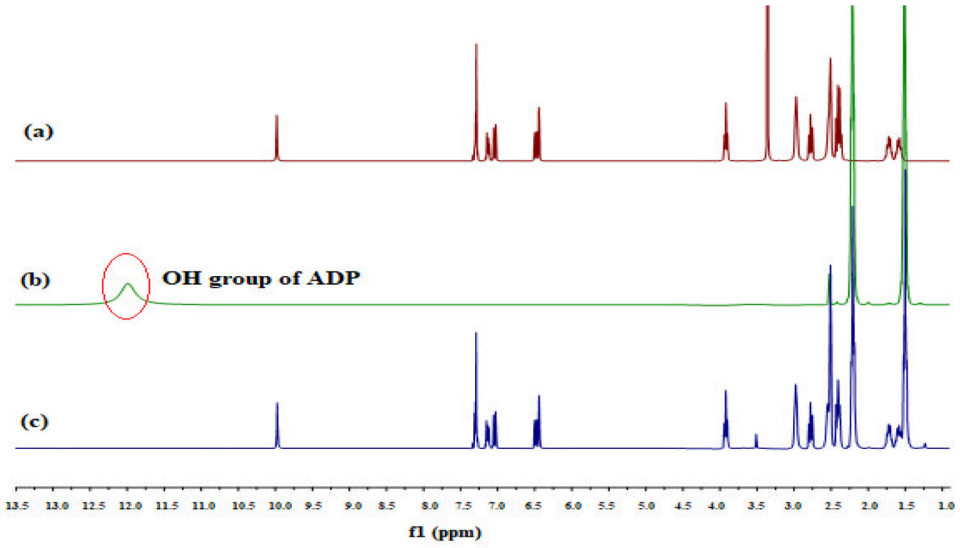

Figure 8.
The ^{1}H NMR spectrum of (a) pure ARP, (b) ADP, and (c) cocrystals.

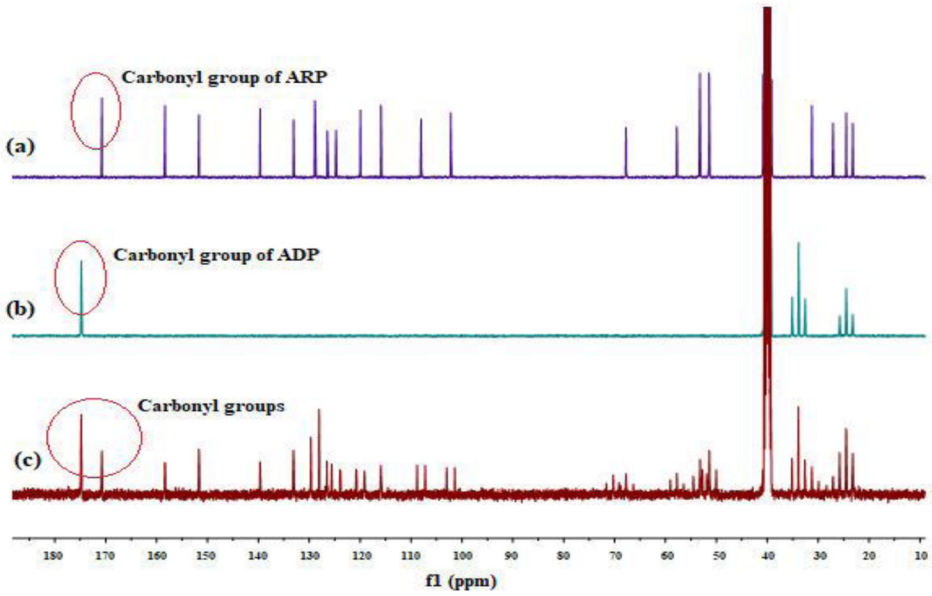

Figure 9.
The ^{13}C NMR spectrum of (a) pure ARP, (b) ADP, and (c) cocrystals.

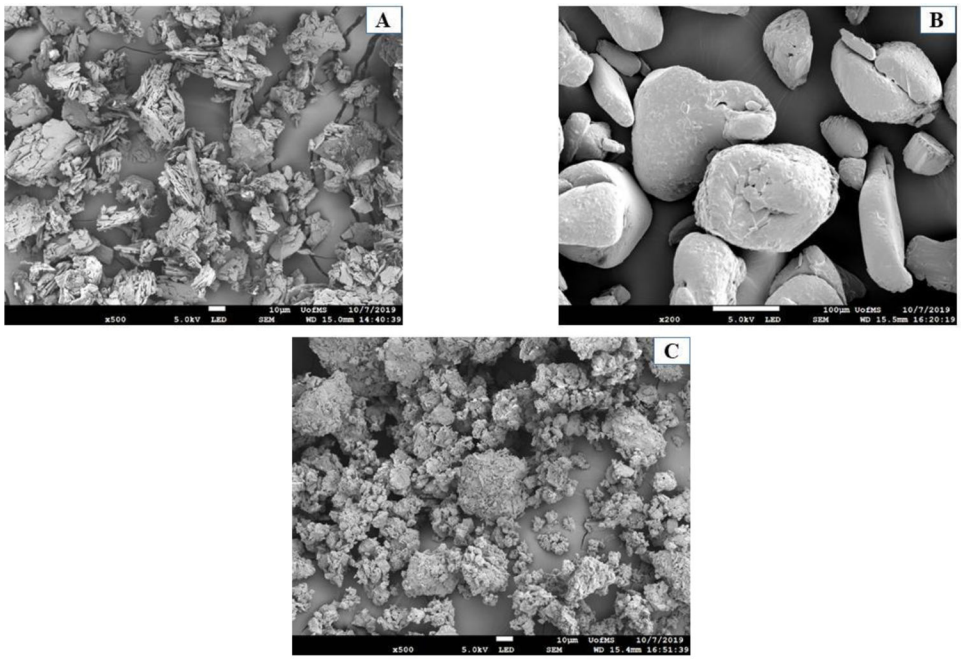

Figure 10.
SEM images of A) ARP, B) ADP, and C) ARP-ADP cocrystals.

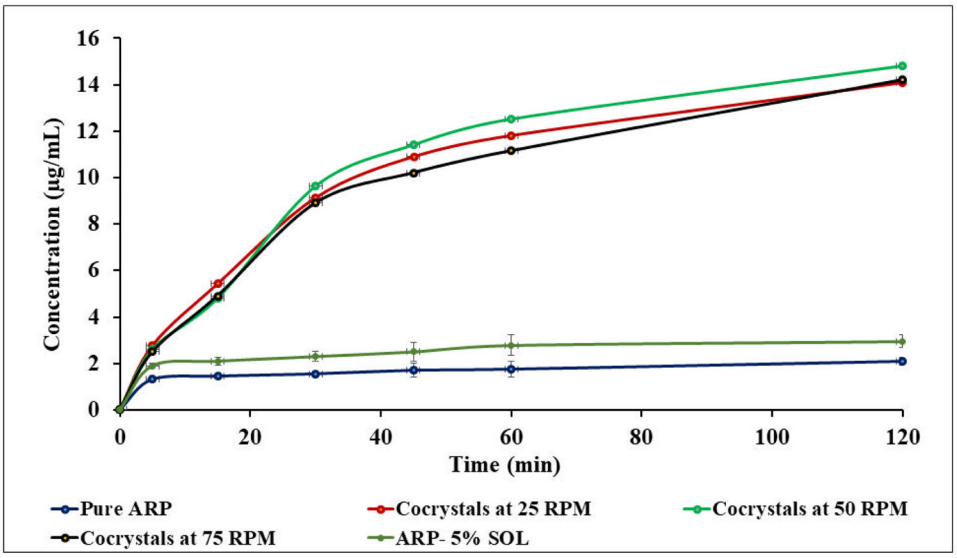

Figure 11.

Dissolution profiles of pure ARP, ARP-5% SOL and cocrystals processed at different screw speeds.

Table 1.

Effect of HME process parameters on the formation of cocrystals.

Formulation code	Temperature (°C)	Screw speed (rpm)	Processing torque (%)	Formation of cocrystals
F1	100	50	30–35	X
F2	115	25		✓
F3	115	50	11–16	✓
F4	115	75		✓
F5	125	50	<10 (Melting of physical blend)	X

Table 2.

Flow properties of pure ARP and cocrystals.

Parameter	Pure ARP	Cocrystals
Bulk density (g/cm3)	0.302 ± 0.017	0.46 ± 0.023
Tapped density (g/cm3)	0.511 ± 0.051	0.766 ± 0.068
Carr's index (%)	41 ± 5.02	24 ± 2.02
Hausner ratio	1.69 ± 0.19	1.31 ± 0.17
True density (g/cm^3)	1.318 ± 0.0009	1.391 ± 0.0003